Available online at www.sciencedirect.com
SCIENCE DIRECT
Journal of Colloid and Interface Science 286 (2005) 400–409
JOURNAL OF Colloid and Interface Science
www.elsevier.com/locate/jcis

Analysis of the response of suspended colloidal soft particles to a constant electric field

J.J. López-García [a], C. Grosse [b,c], J. Horno [a,*]

[a] *Departamento de Física, Universidad de Jaén, Campus Las Lagunillas, Ed. A-3, 23071 Jaén, Spain*
[b] *Departamento de Física, Universidad Nacional de Tucumán, Av. Independencia 1800, 4000 San Miguel de Tucumán, Argentina*
[c] *Consejo Nacional de Investigaciones Científicas y Técnicas, Argentina*

Received 29 October 2004; accepted 13 January 2005

Available online 19 February 2005

Abstract

A network model, originally designed for an electrokinetic study of soft particle suspensions, has been used for an in-depth analysis of the physical behavior of these systems under the action of an externally applied DC electric field. The versatility of the network simulation method used makes it possible to obtain information readily not only about the electrophoretic mobility, but also about any physical variable of interest at all points around the suspended particle: electric potential, ion concentrations, fluid velocity. The field-induced polarization of the double layer is described in terms of the dependence of these and other derived variables (volume charge density, electric field components, ion flux components) on the distance to the membrane–solution interface. In contrast to colloidal suspensions of hard particles, which basically depend on just two parameters (the reciprocal Debye length multiplied by the particle radius, κa, and the zeta potential, ζ), soft particle suspensions require a wider parameter set. First, there are two characteristic diffusion lengths in the system (one inside the membrane and the other in the solution) and two geometrical lengths (the core radius a and the membrane thickness ($b - a$)). Furthermore, there is the fixed charge density inside the membrane (and possibly a surface charge density over the core) that cannot be represented by a ζ potential. Finally, the parameter that characterizes the interaction between the fluid and the permeable membrane, γ, strongly influences the behavior of the system. Dependences on all these parameters (except the geometrical ones) are included in this study.

Keywords: Soft particles; Charged membranes; Spherical particles; Network simulation method; Velocity profiles; DC electric field

1. Introduction

Dielectric and electrokinetic properties of colloidal suspensions are powerful analytical tools in colloidal science, often used for the characterization of colloidal systems [1–3]. This is why many theoretical models relating the different dielectric and electrokinetic properties of suspended particles to the properties of the whole system have been proposed. Among these, the properties of colloidal systems formed by charged insulating spherical particles have a special significance, since they constitute the first approximation to real colloidal suspensions. While these systems have been exhaustively studied in the past century [4–23], in recent years several authors have extended the rigid spherical particle model and associated boundary conditions to more realistic physical situations, e.g., spheroidal particles [24–26], surfaces containing dissociable functional groups [27], amphoteric surfaces [28–30], and surfaces covered with an ion-permeable layer [31–41].

The case of colloidal particles coated with an ion-permeable layer (soft particles) is especially important for the description of bare and polymer-coated latex particles. It can also be used for many biological systems such as plant cells, which have a permeable membrane made of polysaccharides surrounding the cellular membrane, called a cell

* Corresponding author. Fax: +34-953-21-28-38.
E-mail address: jhorno@ujaen.es (J. Horno).

0021-9797/$ – see front matter
doi:10.1016/j.jcis.2005.01.021

wall, that provides and maintains the shape of these cells and serves as a protective barrier [42].

Ohshima [34,37] presented an extensive series of theoretical papers dealing with the electrophoretic mobility and the dielectric properties of soft particles in which approximate analytical expressions were obtained. However, their range of validity is limited by the requirements that $\kappa(b-a) \gg 1$ and $\lambda(b-a) \gg 1$. Here a is the radius of the core, b is the outer membrane radius, κ^{-1} is the Debye length, and λ^2 is the ratio between the drag coefficient of the membrane and the viscosity of the fluid. The solution of the problem in the general case necessarily requires the use of numerical methods. Recent works by Hill et al. [38,39] and by López-García et al. [40,41] provide numerical results for the electrophoretic mobility and the dielectric properties of particles coated with a charged permeable membrane, taking into account the double-layer polarization and without any restriction on the thickness of the membrane, its charge, the number of ion species, etc.

It should be noted that these works are based on different models: a polymer coating with a fuzzy outer boundary in [38,39] and a permeable membrane with sharp outer boundary in [40,41]. Both approaches have advantages and limitations. Hill's model is certainly more general, since it includes a parameter that makes it possible to vary the type of coating continuously from a rather sharp outer boundary (brushlike coating) to segment densities that slowly decay with distance to the core surface. It also simplifies the numerical calculations, since the continuous transition from the coating to the electrolyte solution avoids the necessity of introducing new boundary conditions. On the down side, the extra parameter required to characterize the system complicates the interpretations. This is why, in the results published so far [38,39], only brushlike coatings are considered.

As for López-García's model [40,41], its main advantage is simplicity: the coating is represented just by its segment and charge densities and by its thickness. The outer boundary is perfectly sharp. It also coincides with the representation used by Ohshima in previous theoretical works [34,37], for which limited analytical results exist. From the numerical standpoint, it requires a new set of boundary conditions to be satisfied at the coating–electrolyte solution interface. Actually, the existing expression [37] for the force balance boundary condition had to be corrected in [40], including an additional term corresponding to the force exerted by the liquid on the core of the moving particle.

However, neither of the existing numerical works analyze fundamental questions such as how the ionic concentrations are influenced by the field, or what is the geometry of the fluid velocity profiles around the particle and inside the coating. The answer to these questions is required for a complete understanding of the studied system. The aim of this work is to use the network model already designed [40] to increase our knowledge of the response of a suspended spherical particle coated with a charged permeable membrane to a DC electric field.

2. Theory

We consider a rigid insulating particle of radius a, absolute permittivity ε_{in}, and fixed surface charge density σ_0. The particle is coated with a permeable membrane with external radius b bearing a fixed homogeneous charge density ρ^v, and is immersed in an arbitrary electrolyte solution formed by m ionic species with charge numbers z_i ($i = 1, \ldots, m$), bulk concentrations c_i^∞ (mol/m^3), and diffusion coefficients D_i. The electrolyte solution is incompressible and has a viscosity η, a mass density ρ_{f}, and an absolute permittivity ε_{ex}. While the membrane is permeable to the electrolyte solution, the fluid flow inside it exerts a frictional drag on the polymer segments that is characterized by a drag coefficient γ.

The standard set of equations governing the dynamics of this system was presented in detail in [40]. They are written here for sake of completeness and to specify the nomenclature:

$$c_i(\mathbf{r})\mathbf{v}_i(\mathbf{r}) = -D_i\nabla c_i(\mathbf{r}) - \frac{z_i e D_i}{kT} c_i(\mathbf{r})\nabla\phi(\mathbf{r}) + c_i(\mathbf{r})\mathbf{v}(\mathbf{r}), \tag{1}$$

$$\nabla\cdot\big[c_i(\mathbf{r})\mathbf{v}_i(\mathbf{r})\big] = 0, \tag{2}$$

$$\nabla^2\phi(\mathbf{r}) = \begin{cases} -\dfrac{eN_{\text{A}}\sum_{i=1}^m z_i c_i(\mathbf{r})}{\varepsilon_{\text{ex}}} & \text{if } r > b, \\ -\dfrac{eN_{\text{A}}\sum_{i=1}^m z_i c_i(\mathbf{r})}{\varepsilon_{\text{ex}}} - \dfrac{\rho^v}{\varepsilon_{\text{ex}}} & \text{if } a \leqslant r \leqslant b, \end{cases} \tag{3}$$

$$-\eta\nabla^2\mathbf{v}(\mathbf{r}) + \nabla P(\mathbf{r}) + eN_{\text{A}}\left[\sum_{i=1}^m z_i c_i(\mathbf{r})\right]\nabla\phi(\mathbf{r}) + \rho_{\text{f}}\big[\mathbf{v}(\mathbf{r})\cdot\nabla\big]\mathbf{v}(\mathbf{r}) = \begin{cases} 0 & \text{if } r > b, \\ -\gamma\mathbf{v}(\mathbf{r}) & \text{if } a \leqslant r \leqslant b, \end{cases} \tag{4}$$

$$\nabla\cdot\mathbf{v}(\mathbf{r}) = 0. \tag{5}$$

In these equations, $\mathbf{v}_i$ and c_i are the velocity and the concentration (in mol/m^3) of the ionic species i, $\phi(\mathbf{r})$ is the electric potential, $\mathbf{v}(\mathbf{r})$ the fluid velocity, and $P(\mathbf{r})$ the pressure. The constant e represents the elementary charge, while k, T, and N_{A} are the Boltzmann constant, the absolute temperature, and the Avogadro number. In the present study it is assumed for simplicity that the dielectric constant of the membrane phase is the same as that of the liquid phase, as should approximately be the case for polymer-coated particles. For other types of membranes, for which the difference between these constants is appreciable, the ion-partitioning effect that arises from the Born energy needs to be considered as is done, for example, in Ref. [43]. Also, for mathematical simplicity, the diffusion coefficients of all the ionic species are considered to have the same values inside the membrane and in the solution.

This equation system is first simplified by combining Eqs. (1) and (2) to eliminate the ion velocities. The pressure is then eliminated by taking the curl of Eq. (4) and introduc-

ing the vorticity, defined as

$$\boldsymbol{\Omega}(\mathbf{r}) = \nabla \times \mathbf{v}(\mathbf{r}). \tag{6}$$

The resulting equations are first solved in equilibrium and then under the action of a weak DC electric field, E_a. The perturbed equations are linearized with respect to the applied field, referring the perturbed variables to their equilibrium values (upper index 0),

$$c_i(\mathbf{r}) = c_i^0(r) + \delta c_i(\mathbf{r}), \tag{7}$$

$$\phi(\mathbf{r}) = \phi^0(r) + \delta\phi(\mathbf{r}), \tag{8}$$

and keeping in the final equations only terms that are linear in the perturbations.

The boundary conditions used have been analyzed at length in [40]:

- Inside the core the electric field is uniform.
- At the surface of the core the electric potential and the normal component of the displacement vector are continuous. The fluid velocity and the radial component of the ion velocities vanish.
- At the membrane–electrolyte solution interface, the electric potential, the normal component of the displacement vector, the fluid velocity, the ionic concentrations, the ionic velocities, the vorticity, and the pressure are continuous.
- Far from the particle, the electric potential reduces to that of the applied field and the fluid velocity to minus the electrophoretic velocity. The perturbations of the ionic concentrations and the vorticity vanish.
- The total force acting on the particle vanishes.

For computational reasons, the equations are first transformed using a new set of dimensionless variables. They are then discretized and the network circuits designed in a way similar to that in [40]. After the network model is constructed, an electric circuit simulation program is finally used to obtain the values of the desired quantities, mainly potentials at different points of the circuit, i.e., of the membrane and surrounding electrolyte solution. We found the PSPICE package most suitable for this purpose.

3. Results and discussion

Although the equilibrium properties of the system have been extensively studied in previous papers [30,34–36], we briefly describe the more important aspects needed to understand the behavior of the system out of equilibrium. Fig. 1 represents the reduced equilibrium potential (Fig. 1a) and concentration (Fig. 1b) profiles for different values of the membrane charge and for an uncharged core ($\sigma_0 = 0$). It was shown in previous papers [30,35] that the charge of the core merely raises or lowers the electrical potential in the close vicinity to its surface, leaving unaltered the electric potential

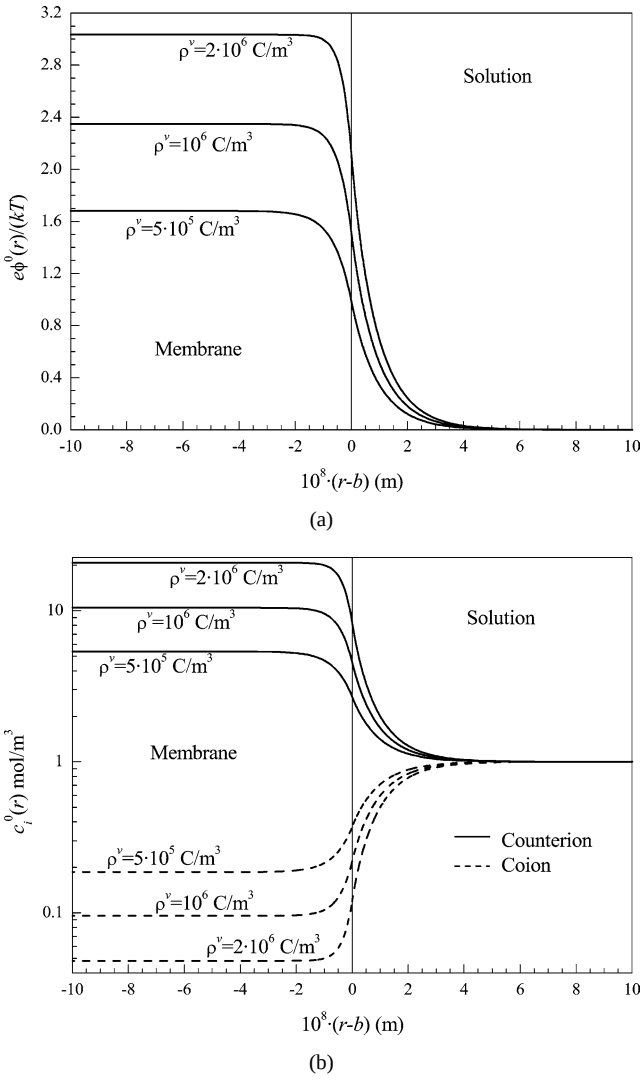

Fig. 1. Equilibrium profiles of the reduced electric potential (a) and the ionic concentrations (b) for the parameter values shown in Table 1 and the indicated volume charge densities.

and, therefore, the ion concentrations in the remaining space. As expected, when the fixed charge of the membrane grows, the reduced equilibrium potential and the counterion concentration also grow, while the co-ion concentration decreases. It is important to note that when the membrane thickness is larger than the Debye length (as is the case in Fig. 1), an electroneutral region appears inside the membrane, in which the electric potential and the ionic concentrations remain constant.

In what follows we shall examine the dependence of the field-induced changes of the electric potential, ion concentrations, volume charge density, and fluid velocity profiles with the parameters of the system. The data set used in all calculations, except when indicated, is given in Table 1, where the parameter λ is defined as $\lambda \equiv \gamma/\eta$.

It should be noted that the value of the applied electric field E_a is set to 1 V/m. Since the theory is based on the assumption that all the field-induced quantities are linear in

Table 1
Parameter values used in the figures, except where indicated

$\varepsilon_{ex} = 80\varepsilon_0$	$\varepsilon_{in} = 2\varepsilon_0$	$T = 298$ K	$a = 10^{-6}$ m
$b = 1.1 \times 10^{-6}$ m	$m = 2$	$z_1 = 1$	$z_2 = -1$
$c_1^\infty = 10^{-3}$ M	$c_2^\infty = 10^{-3}$ M	$D_1 = 2 \times 10^{-9}$ m^2/s	$D_2 = 2 \times 10^{-9}$ m^2/s
$\rho^v = 10^6$ C/m^3	$\eta = 0.89 \times 10^{-3}$ poise	$\lambda(b-a) = 10^4$	$E_a = 1$ V/m

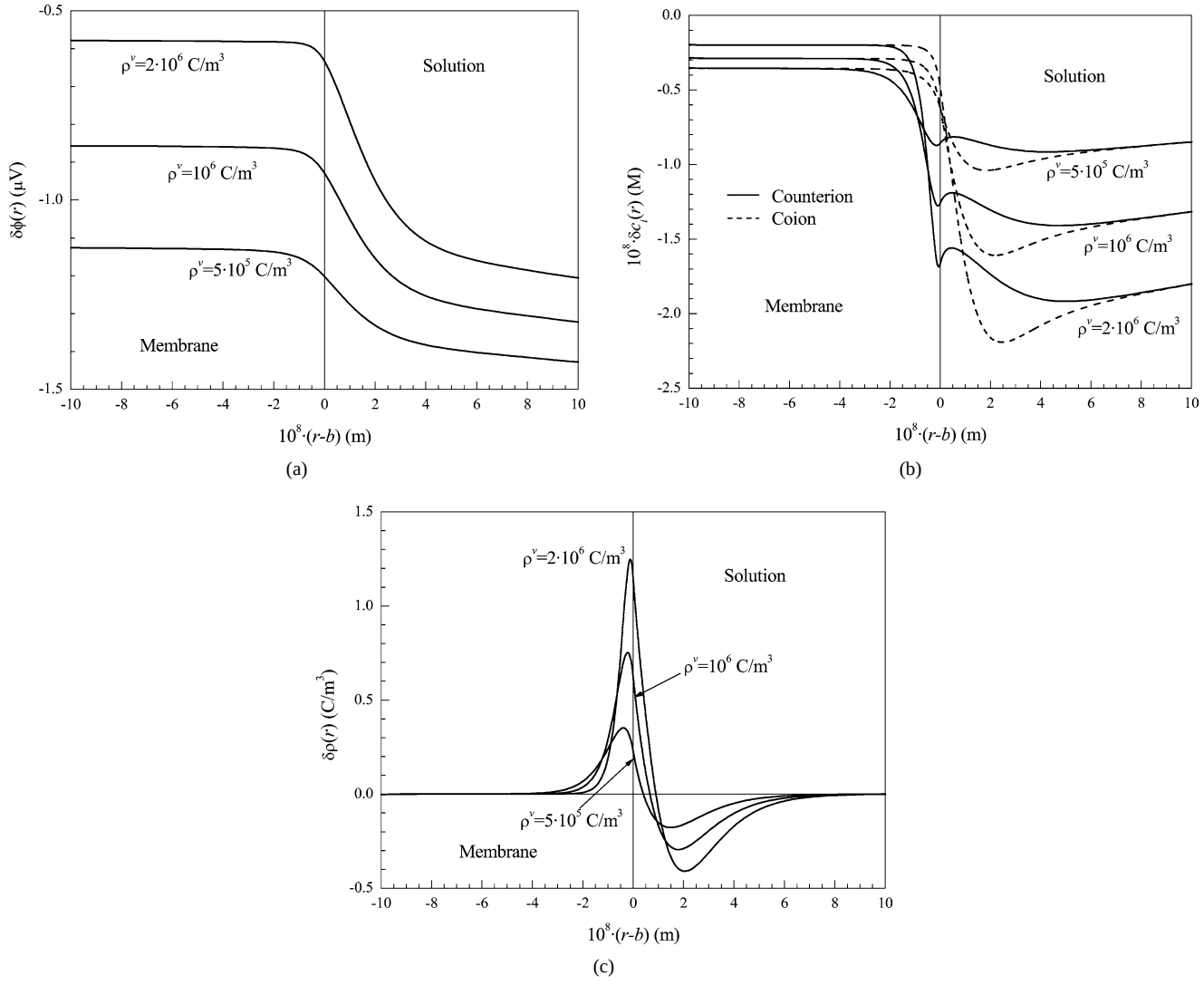

Fig. 2. Perturbation profiles of the electric potential (a), of the ionic concentrations (b), and of the volume charge density (c), for the parameter values shown in Table 1 and the indicated volume charge densities.

E_a, setting its value to 1 V/m is equivalent to using any other value and dividing the results by E_a.

3.1. Dependence on the fixed charge density

Fig. 2 shows the perturbation profiles of the electric potential $\delta\phi(r)$ (Fig. 2a), of the co-ion and counterion concentrations $\delta c_1(r)$ and $\delta c_2(r)$ (Fig. 2b), and of the volume charge density (Fig. 2c), calculated on the symmetry axis ($\theta = 0$) for the indicated membrane charge densities. Outside the membrane, the concentration changes are very close to those corresponding to bare latex particles [44]: the electrolyte concentration decreases over a distance on the order of a particle radius and up to a few Debye lengths from the membrane–electrolyte solution interface. Close to the particle, the co-ion concentration change decreases faster than that of counterions, leading to a negative volume charge density, Fig. 2b. Less than one Debye length from the interface the two curves intersect, which corresponds to a positive charge density that extends inside the membrane, Fig. 2c. The sharp minima just inside the membrane of the curves corresponding to counterions arise because curves with a

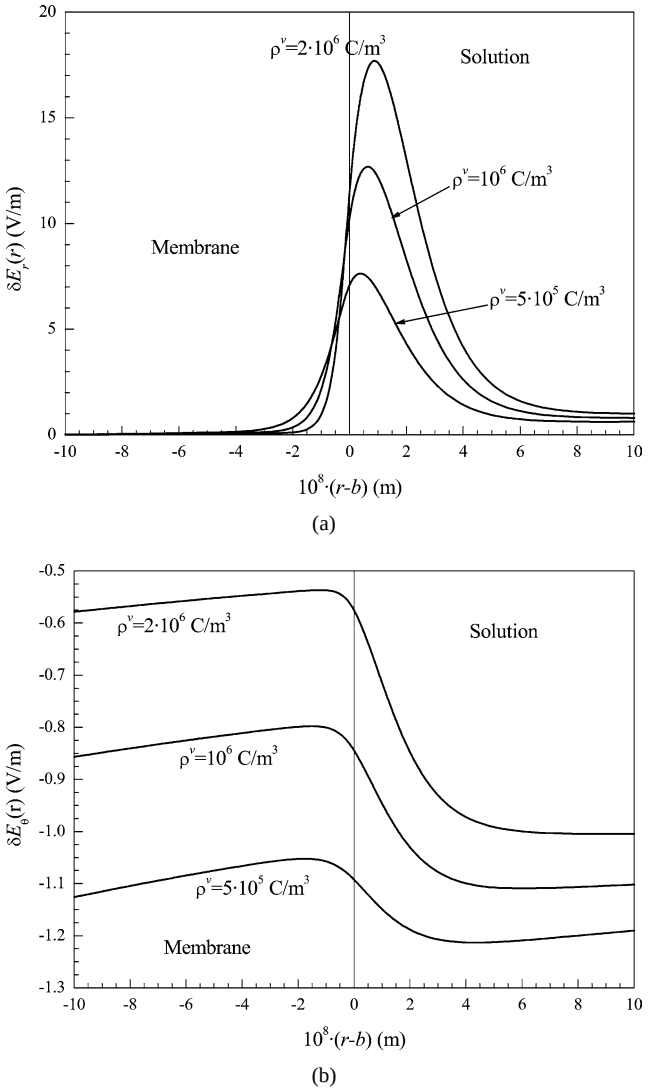

Fig. 3. Perturbation profiles of the radial component (a) and of the tangential component (b) of the electric field, for the parameter values shown in Table 1 and the indicated volume charge densities.

negative slope inside the membrane must join curves with a positive slope outside it. It should be noted that this positive slope is also present in bare particles, as it has already been discussed [44,45].

The inner part of the membrane, which is electroneutral in equilibrium, Fig. 1, remains electroneutral when a stationary field is applied, Fig. 2c. This stationary state is attained with counterion and co-ion changes inside the membrane that are lower (in absolute value) the higher is the fixed charge density, Fig. 2b. This dependence is a result of the electric shielding of the inner part of the membrane by the surface conductivity of the particle, as can be seen in Fig. 3. This figure represents the profiles of the radial (Fig. 3a) and tangential (Fig. 3b) nonequilibrium electric field components, calculated on the symmetry axis for $\delta E_r(r)$ and on the equator for $\delta E_\theta(r)$. As shown in Fig. 3a, the radial component of electric field tends to a limiting value of 1 V/m far from the particle, has a very large value near the membrane–electrolyte solution interface (where the field-induced charge density changes sign), and decreases to very low values inside the membrane. In contrast, the tangential component tends to a limiting value of −1 V/m far from the particle, as expected, it has a much weaker variation with the radial coordinate, and its absolute value decreases with the fixed charge in the membrane, Fig. 3b.

The dependencies of the different variables on the radial coordinate inside the membrane can easily be calculated using the condition of electroneutrality both in equilibrium and with an applied field, together with the assumption that the convective flow is negligible (as is the case for the value $\lambda(b-a)=10^4$ used in Figs. 1–4). Under these conditions,

$$\delta c_1(r) = \delta c_2(r) = \delta c,$$

while Eq. (3) shows that the potential change is a solution of the Laplace equation,

$$\delta\phi(r) = -Ar + \frac{B}{r^2}, \tag{9}$$

so that the ion flows, derived from Eq. (1), have the form

$$\begin{aligned}\mathbf{j}_i(r) &= -c_i^0 D_i \nabla\left[\frac{\delta c}{c_i^0} + \frac{z_i e}{kT}\delta\phi(r)\right] \\ &= -c_i^0 D_i \nabla\left[\frac{\delta c}{c_i^0} + \frac{z_i e}{kT}\left(-Ar + \frac{B}{r^2}\right)\right].\end{aligned}$$

Using the condition that the radial flow must vanish on the surface of the core leads to

$$B = -\frac{a^3 A}{2},$$

so that the radial and tangential components of the electric field and of the ion flows inside the membrane can be written as

$$\delta E_r(r) = A\left(1 - \frac{a^3}{r^3}\right), \tag{10}$$

$$\delta E_\theta(r) = -A\left(1 + \frac{a^3}{2r^3}\right), \tag{11}$$

$$j_{ir}(r) = c_i^0 D_i \frac{z_i e A}{kT}\left[1 - \frac{a^3}{r^3}\right], \tag{12}$$

$$j_{i\theta}(r) = c_i^0 D_i\left[\frac{\delta c}{c_i^0}\frac{1}{r} - \frac{z_i e A}{kT}\left(1 + \frac{a^3}{2r^3}\right)\right]. \tag{13}$$

Equation (10) explains the growth with r of the radial field in the membrane (barely visible in Fig. 3a), while Eq. (11) explains the negative sign and the decrement with r of the absolute value of the tangential field component, Fig. 3b. Moreover, the strong variation of δE_θ with the fixed charge density is a direct consequence of the variation of $\delta\phi$ with ρ^v, Eq. (9) and Fig. 2a.

The radial and tangential components of the ion flows are represented in Fig. 4. Inside the membrane, the flow of counterions is much stronger than that of co-ions, mainly due to

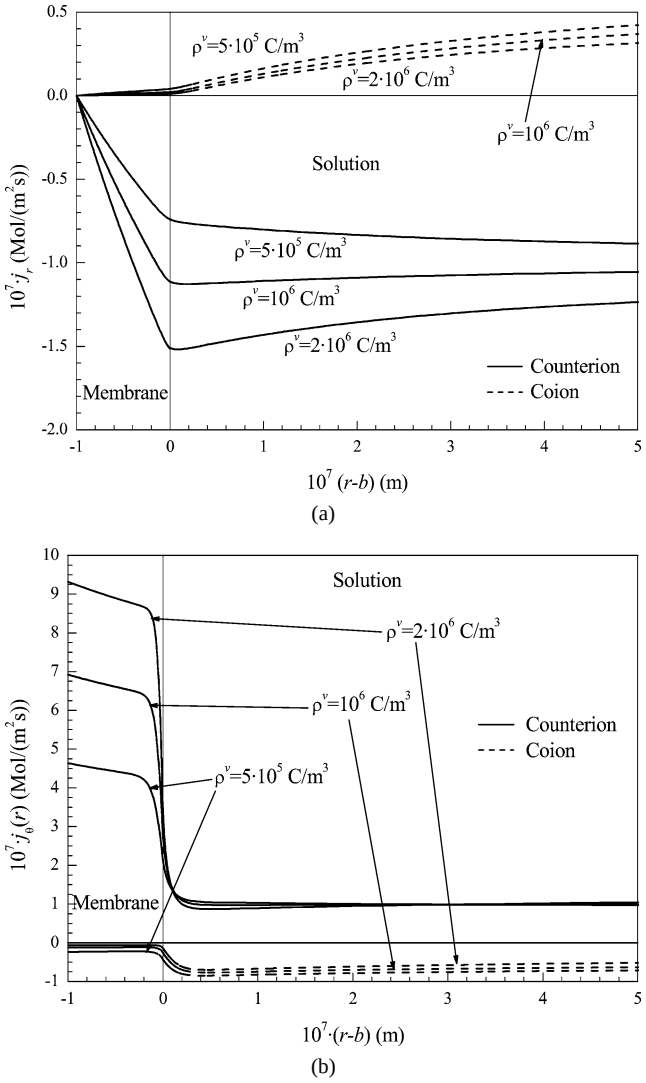

Fig. 4. Perturbation profiles of the radial component (a) and of the tangential component (b) of the ionic fluxes, for the parameter values shown in Table 1 and the indicated volume charge densities.

their much higher equilibrium concentration, Fig. 1b. Moreover, the counterion flow strongly increases with the fixed charge of the particle, while the co-ion flow is almost independent of ρ^v. This behavior is easily explained with the help of Eqs. (12) and (13). For counterions, both c_2^0 and A increase when the fixed charge density increases, leading to a strong increase of both components of the ion flows (for the tangential component, the first addend on the right-hand side of Eq. (13) is small as compared to the second, in view of the high value of c_2^0). In contrast, for co-ions, c_1^0 decreases with the fixed charge density while A increases, so that the radial component of the flow, Eq. (12), remains approximately constant. As for the tangential component, the second addend on the right-hand side of Eq. (13) remains approximately constant when the fixed charge increases (c_1^0 decreases while A increases), while the first one decreases in absolute value, Fig. 2b. This last decrement leads to the small variation observed in Fig. 4b.

Outside the membrane, the ion flows are similar to those corresponding to bare charged particles. Far from the particle, the radial flow values tend, in all cases, to minus the corresponding value of the tangential flows, as expected. Moreover, these limiting values are larger for counterions than for co-ions (Fig. 4), since the convective term adds to the electromigration term for counterions, while it subtracts for co-ions:

$$j_{ir}(r\to\infty) = -j_{i\theta}(r\to\infty) = c_i^0\left[\frac{z_i e D_i}{kT}E_a - v_d\right]. \quad (14)$$

Near the particle, at distances on the order of its radius, the radial flow of counterions is much larger than that of co-ions (in absolute value) and the difference increases with the fixed charge value. This is in full agreement with the ion concentration profiles (Fig. 2b), which contribute to increase the radial flow of counterions and decrease that of co-ions.

3.2. Dependence on the drag coefficient

We shall now analyze the effect of changes in the drag coefficient on the behavior of the system. When the parameter λ is lowered, the fluid starts to flow inside the membrane, Fig. 5. For high values of the drag coefficient, the fluid velocity inside the membrane vanishes while, outside the membrane, the velocity profile corresponds to that of a charged rigid particle with radius b. At great distances it tends to the electrophoretic velocity, which has a rather small value, since most of the fixed charge is screened inside the membrane (the reduced surface potential is equal to 1.515). At intermediate values of λ, the tangential component of the velocity inside the membrane presents a plateau, decreases to zero on the surface of the core, and increases on the outer membrane boundary (Fig. 5b). For very low values of the drag coefficient this plateau disappears and the fluid velocity monotonically increases across the membrane. Outside the membrane the velocity decreases to the electrophoretic value, which is much higher than for high drag coefficients, because the electroosmotic flow arises across the whole membrane thickness and not just the external double layer [40].

These changes in the fluid flows have a very strong bearing on the ion flows both inside and outside the membrane, as can be seen by comparing Fig. 6 with Fig. 4. Since changes due to fluid motion have the same sign for both types of ions, the tangential flow of counterions inside the membrane strongly increases, while that of co-ions decreases (in absolute value). The reverse is true for the radial component. Outside the membrane, the most notable change is that for $\lambda(b-a)=1$, the electrophoretic velocity becomes so high that the flow of co-ions changes sign: positive ions outside a positive particle move in the direction opposite to the applied field (in the reference frame of the particle).

The stronger tangential flow of counterions inside the membrane leads to an increment (in absolute value) of the ion concentration changes (Fig. 7a), to an increment of the

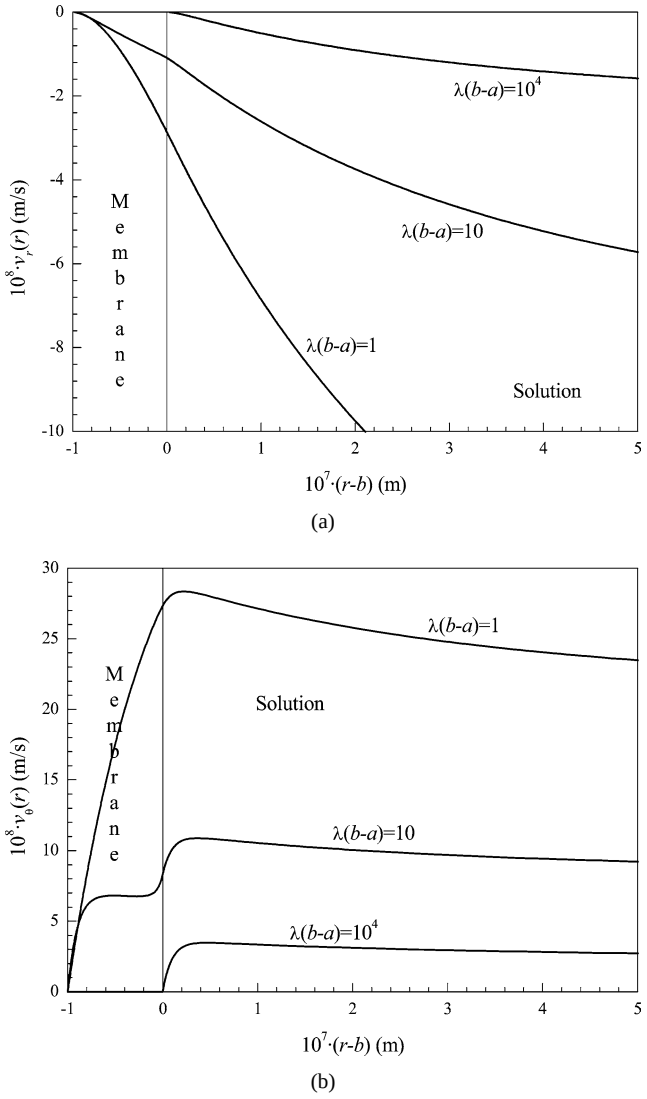

Fig. 5. Perturbation profiles of the radial component (a) and of the tangential component (b) of the fluid velocity, for the parameter values shown in Table 1 and the indicated values of the product $\lambda(b-a)$.

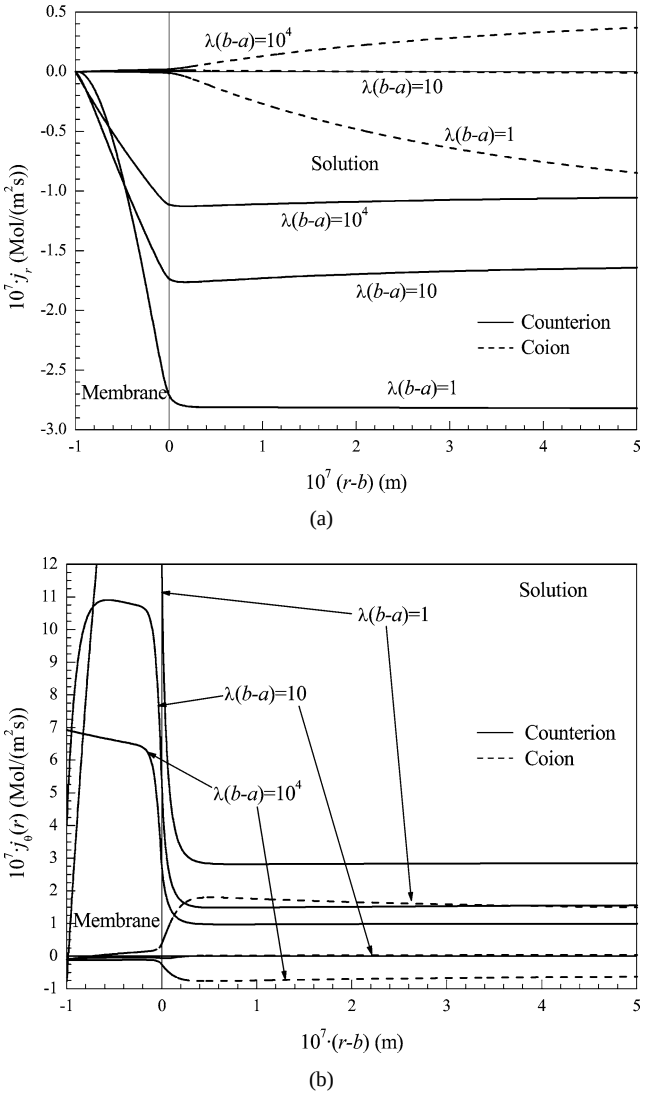

Fig. 6. Perturbation profiles of the radial component (a) and of the tangential component (b) of the ionic fluxes, for the parameter values shown in Table 1 and the indicated values of the product $\lambda(b-a)$.

field-induced charge density (Fig. 7b), and to a corresponding decrement (in absolute value) of the electric potential change (Fig. 7c). It should be noted that for the lowest drag coefficient considered, the potential change inside the membrane is positive, which means that the direction of the tangential field inside the membrane is opposite to that of the applied field.

3.3. Dependence on the electrolyte concentration

An analysis of the influence of the electrolyte concentration on the behavior of the system is complicated by the fact that equilibrium properties are also modified, Fig. 8. This figure shows that the equilibrium potential strongly increases when the electrolyte concentration decreases, keeping the fixed charge density constant, and that the double layer thickness outside the membrane increases, as expected. However, the double layer thickness inside the membrane remains approximately constant, since it mainly depends on the density of counterions, which barely changes [30]. Therefore, in order to attain a situation where the electroneutrality of the membrane is lost, both the electrolyte concentration and the fixed charge density must be lowered. This is illustrated in Fig. 9, which shows the reduced equilibrium potential and ion concentration profiles calculated keeping the quotient ρ^v/c_i^∞ at a very low constant value of 5×10^4 C/(m^3 M). As can be seen, under these conditions the membrane ceases to be electroneutral at the lowest concentration (Fig. 9a). Moreover, Fig. 9b shows that the double layer thickness increases both inside and outside the membrane when the electrolyte concentration is lowered.

Finally, Fig. 10 shows the corresponding field-induced charge density profiles. In contrast to Fig. 2c, the field-induced volume charge calculated at the lowest electrolyte

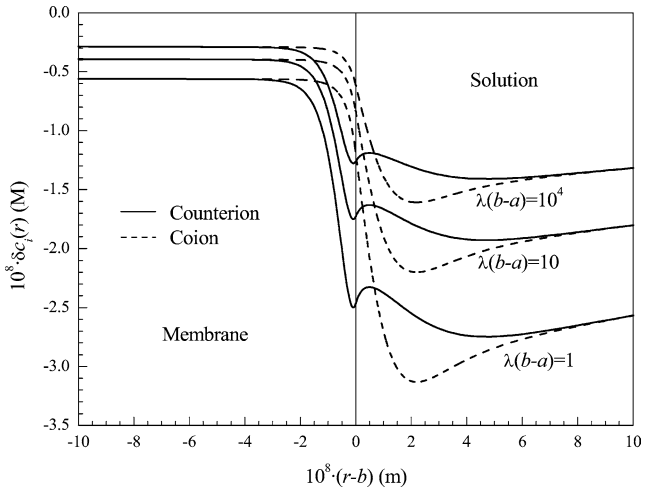

(a)

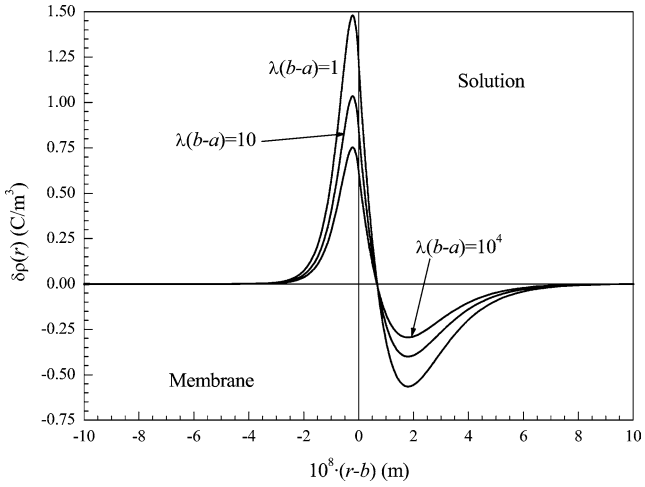

(b)

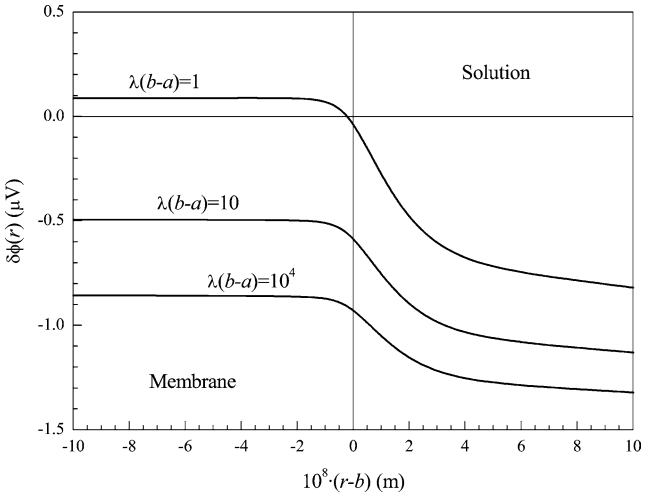

(c)

Fig. 7. Perturbation profiles of the ionic concentrations (a), of the volume charge density (b), and of the electric potential (c) for the parameter values shown in Table 1 and the indicated values of the product $\lambda(b-a)$.

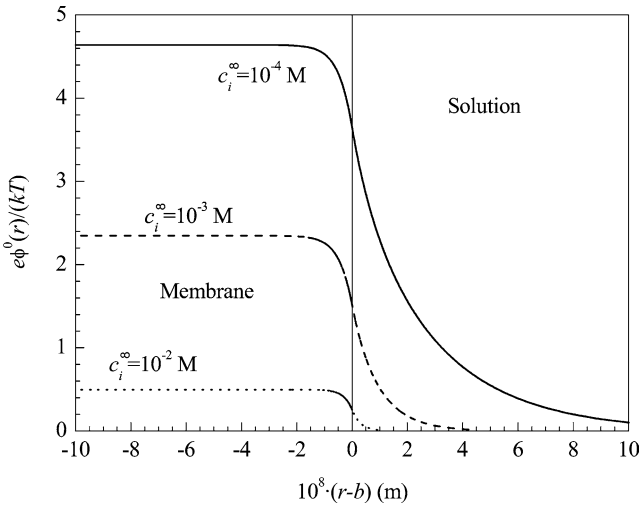

Fig. 8. Equilibrium profiles of the reduced electric potential for the parameter values shown in Table 1 and the indicated values of the ionic concentrations in the solution.

concentration is positive over almost all the thickness of the membrane, not just near its outer boundary. On the contrary, the electroneutrality of the central part of the membrane is preserved for the highest electrolyte concentration and, in this last case, a negative charge density appears close to the surface of the core. This Maxwell–Wagner type volume charge is due to the hypothesis that the core is insulating, so that it should be present in all cases. However, it is only visible in Fig. 10 because of the low values of the fixed charge density, which lead to low surface conductivity values (Fig. 9b) that minimize the shielding of the core.

4. Conclusion

Model colloidal suspensions of charged soft particles are important systems that are useful for the representation of many biological particles, polymer-coated latex particles, and even real uncoated particles. However, these are complex systems, defined by a series of parameters in addition to the usual ones that characterize hard particle suspensions, namely the membrane thickness, membrane drag coefficient, and fixed charge density in the membrane. This last parameter must be specified instead of the ζ potential, which is ill defined for soft particles [40,46]. Because of this complexity, a detailed understanding of the behavior of these systems is relatively difficult. We hope that this work will be helpful in this aspect.

The dielectric and electrokinetic properties of suspensions of hard particles are mainly dependent on their charge and on the value of the product κa. In addition to this, soft particle suspensions also depend on the values of the products $\lambda(b-a)$ and $\kappa_{\mathrm{mem}}(b-a)$ (κ_{mem} is a reciprocal Debye length related to the equilibrium counterion density in the membrane rather than to the ion densities far from the particle [30]). For large $\lambda(b-a)$ values, the fluid barely moves

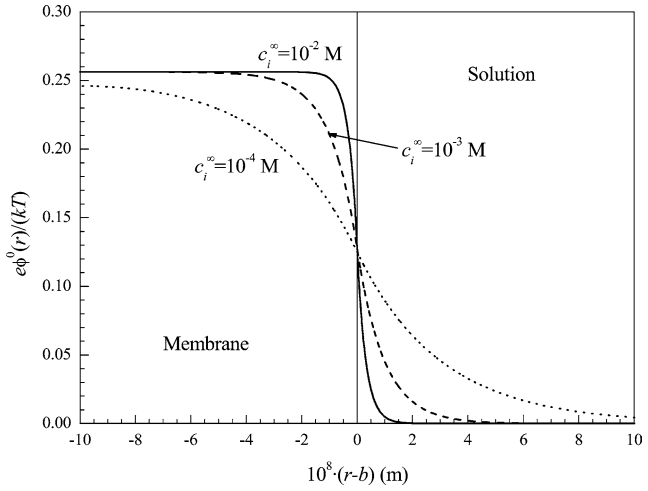

Fig. 9. Equilibrium profiles of the reduced electric potential (a) and the ionic concentrations (b) for the indicated values of the ionic concentrations in the solution and keeping constant the quotient ρ^v/c_i^∞ at a very low value of 5×10^4 C/(m^3 M). Remaining parameters are given in Table 1.

inside the membrane, while, for large $\kappa_{\text{mem}}(b-a)$, the membrane is electroneutral both in equilibrium and with an applied field. The behavior of the system is greatly simplified when both conditions are met, since then, the electrokinetic equation system can be analytically solved inside the membrane.

The field-induced charge density outside the membrane is similar to that for bare particles, but it now extends inside the membrane. It grows with the fixed charge density, partially shielding the membrane, so that the higher the fixed charge, the lower the field-induced ion density changes and electric field inside the membrane. However, the counterion flow increases with the fixed charge.

Low $\lambda(b-a)$ values lead to a strong electroosmotic flow inside the membrane, which greatly increases the convective flow outside the particle and its electrophoretic mobility. Actually, the electrophoretic velocity of the soft particle

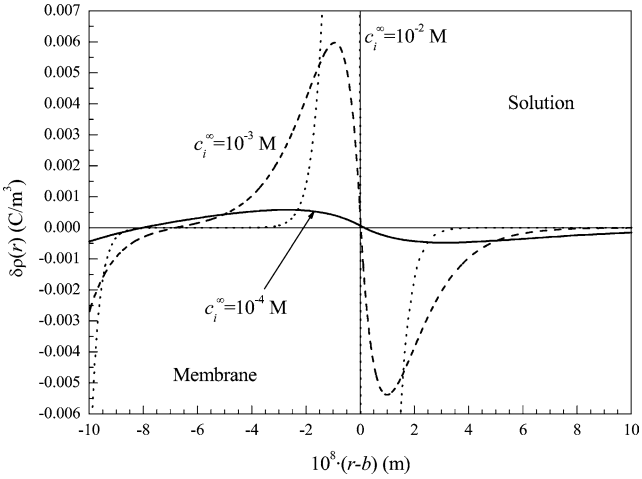

Fig. 10. Perturbation profiles of the volume charge density for the indicated values of the ionic concentrations in the solution and keeping constant the quotient ρ^v/c_i^∞ at a very low value of 5×10^4 C/(m^3 M). Remaining parameters given in Table 1.

can become higher than the electromigration velocity of the ions in the electrolyte solution. Fluid flow inside the membrane also increases the field-induced charge density and, correspondingly, decreases the field-induced electric potential. This decrement can be so large as to reverse the direction of the electric field inside the membrane.

Keeping constant the membrane thickness, a low value of the product $\kappa_{\text{mem}}(b-a)$ can only be attained by reducing both the fixed charge density and the electrolyte concentration, since the counterion concentration inside the membrane is almost independent of the electrolyte concentration. Under these conditions, electroneutrality inside the membrane is lost both in equilibrium and with an applied field, when a field-induced charge density extends across the membrane. Furthermore, the electric shielding of the inner volume of the membrane is greatly reduced, leading to a significant Maxwell–Wagner type charge density distribution over the surface of the core.

Acknowledgments

Financial support by the Ministerio de Ciencia y Tecnología, Spain, under project BFM2003-4856 and by Consejo de Investigaciones de la Universidad Nacional de Tucumán, Agencia Nacional de Promoción Científica y Tecnológica, and Consejo Nacional de Investigaciones Científicas y Técnicas, Argentina, is gratefully acknowledged.

References

[1] W.B. Russell, D.A. Saville, W.R. Schowalter, Colloidal Dispersions, Cambridge Univ. Press, Cambridge, UK, 1995.
[2] R.J. Hunter, Foundations of Colloid Science, vol. I, Oxford Univ. Press, London, 1995.

[3] J. Lyklema, Fundamentals of Colloid and Interface Science, vol. II, Solid/Liquid Interfaces, Academic Press, London, 1995.
[4] G. Schwarz, J. Phys. Chem. 66 (1962) 2636.
[5] S.S. Dukhin, V.N. Shilov, Dielectric Phenomena and the Double Layer in Disperse Systems and Polyelectrolytes, Kerter Publishing House, Jerusalem, 1974.
[6] W.C. Chew, P.N. Sen, J. Chem. Phys. 77 (1982) 4683.
[7] R.W. O'Brien, Adv. Colloid Interface Sci. 16 (1982) 281.
[8] M. Fixman, J. Chem. Phys. 78 (1983) 1483.
[9] M. Mandel, T. Odijk, Ann. Rev. Phys. Chem. 35 (1984) 75.
[10] C. Grosse, K.R. Foster, J. Phys. Chem. 91 (1987) 3073.
[11] E.H.B. DeLacey, L.R. White, J. Chem. Soc. Faraday Trans. 2 77 (1981) 2007.
[12] C.S. Mangelsdorf, L.R. White, J. Chem. Soc. Faraday Trans. 2 93 (1997) 3145.
[13] J.J. López-García, J. Horno, F. González-Caballero, C. Grosse, A.V. Delgado, J. Colloid Interface Sci. 228 (2000) 95.
[14] H.P. Schwan, G. Schwarz, J. Maczuk, H. Pauly, J. Phys. Chem. 66 (1962) 2626.
[15] C. Ballario, A. Bonincontro, C. Cametti, J. Colloid Interface Sci. 54 (1975) 415.
[16] S. Sasaki, A. Ishikawa, T. Hanai, Biophys. Chem. 14 (1981) 45.
[17] M.M. Springer, A. Korteweg, J. Lyklema, J. Electroanal. Chem. 153 (1983) 55.
[18] K.-H. Lim, E.I. Franses, J. Colloid Interface Sci. 110 (1986) 201.
[19] L.A. Rosen, D.A. Saville, Langmuir 7 (1991) 36.
[20] G. Blum, H. Maier, F. Sauer, H.P. Schwan, J. Phys. Chem. 99 (1995) 780.
[21] C. Grosse, M. Tirado, W. Pieper, R. Pottel, J. Colloid Interface Sci. 205 (1998) 26.
[22] A.V. Delgado, F. González-Caballero, F.J. Arroyo, F. Carrique, S.S. Dukhin, I.A. Razilov, Colloids Surf. A 131 (1998) 95.
[23] M. Minor, H.P. van Leeuwen, J. Lyklema, J. Colloid Interface Sci. 206 (1998) 397.
[24] R.W. O'Brien, D.N. Ward, J. Colloid Interface Sci. 121 (1988) 402.
[25] B.J. Yoon, S. Kim, J. Colloid Interface Sci. 128 (1989) 275.
[26] H.J. Keh, T.Y. Huang, J. Colloid Interface Sci. 160 (1993) 354.
[27] B. Niham, V.A. Parsegian, J. Theor. Biol. 31 (1971) 405.
[28] D.Y.C. Chan, T.H. Healy, J.W. Perram, L.R. White, J. Chem. Soc. Faraday Trans. 1 71 (1975) 1046.
[29] D. Chan, T.H. Healy, L.R. White, J. Chem. Soc. Faraday Trans. 1 72 (1976) 2844.
[30] J.J. López-García, C. Grosse, J. Horno, J. Colloid Interface Sci. 254 (2002) 287.
[31] R.W. Wunderlich, J. Colloid Interface Sci. 88 (1982) 385.
[32] S. Levine, M. Levine, K.A. Sharp, D.E. Brooks, Biophys. J. 42 (1983) 127.
[33] K.A. Sharp, D.E. Brooks, Biophys. J. 47 (1985) 563.
[34] H. Ohshima, J. Colloid Interface Sci. 163 (1994) 474.
[35] J.J. López-García, J. Horno, C. Grosse, Phys. Chem. Chem. Phys. 3 (2001) 3754.
[36] D.A. Saville, J. Colloid Interface Sci. 222 (2000) 137.
[37] H. Ohshima, J. Colloid Interface Sci. 228 (2000) 190.
[38] R.J. Hill, D.A. Saville, W.B. Russel, J. Colloid Interface Sci. 258 (2003) 56.
[39] R.J. Hill, D.A. Saville, W.B. Russel, J. Colloid Interface Sci. 263 (2003) 478.
[40] J.J. López-García, C. Grosse, J. Horno, J. Colloid Interface Sci. 265 (2003) 327.
[41] J.J. López-García, C. Grosse, J. Horno, J. Colloid Interface Sci. 265 (2003) 341.
[42] H. Ohshima, K. Furusawa, Electrical Phenomena at Interfaces: Fundamentals, Measurement and Applications, Dekker, New York, 1998, ch. 27.
[43] J.J. López-García, C. Grosse, J. Horno, J. Colloid Interface Sci. 268 (2003) 371.
[44] J.J. López-García, J. Horno, A.V. Delgado, F. González-Caballero, J. Phys. Chem. B 103 (1999) 297.
[45] S.E. Pedrosa, C. Grosse, J. Colloid Interface Sci. 219 (1999) 37.
[46] H. Ohshima, in: A.T. Hubbard (Ed.), Encyclopedia of Surface and Colloid Science, vol. 2, Dekker, New York, 2002.